 doi:10.20944/preprints201803.0140.v1

Article

3D finite element analysis of Laser Surface Glazing to investigate temperature effects on surface of Ti64 alloy

Israt Rumana Kabir [1]*, Danqing Yin [2], Nusrat Tamanna [1] and Sumsun Naher [1]*

[1] Department of Mechanical Engineering and Aeronautics, City, University of London, EC1V 0HB, UK
[2] Department of Material Processing Engineering, Henan University of Science and Technology, 263 Kaiyuan Avenue, Luoyang, China
* Correspondence: israt.kabir.1@city.ac.uk; sumsun.naher.1@city.ac.uk; Tel.:+447849920755

Abstract: Ti64 alloy plays a significant role in the biomedical applications such as bioimplants for its excellent biocompatibility. Its usage can be further extended by improving the surface hardness and wear resistance. In this respect, laser surface glazing (LSG), an advanced surface modification technique, is very useful which can produce thin hardened surface layer and strong metallurgical bonding. Investigation of temporal and spatial temperature distributions of laser glazed surface of materials are essential because temperature plays significant role in achieving required surface properties. Therefore, in this study, a 3D Finite element analysis has been developed to perform transient thermal analysis of LSG for Ti64 alloy. The model investigated temperature distribution, depth of modified zone and heating and cooling. The results show that the peak temperature is attained 2095 K for 300 W laser power, 0.2 mm beam width and 0.15 ms residence time. Since this temperature is above the melting point (1933 K) of Ti64 alloy, the melt depth is calculated 22.5 μm. Furthermore, from the simulation results, the average heating and cooling rates are estimated 1.19×10^{7} Ks^{-1} and 2.71×10^{6} Ks^{-1} respectively which indicate the presence of hard phases in the modified zone.

Keywords: Laser surface glazing; Ti6Al4V alloy; FEA; thermal model; biomedical application; heating and cooling rates; depth of modified zone; hardness; wear resistance

1. Introduction

Since 1930, Ti64 (widely known as Ti6Al4V) alloy is introduced as a bio-implants material [1] for its high strength-to-weight ratio, good corrosion resistance [2–4] and better ability of joining bones with implants (known as Osseo-integration) [5]. These properties make Ti64 alloy preferable as bone and dental implants [6,7], over the other biocompatible metallic materials such as 316L stainless steel, Cobalt and Vanadium steels [1]. However, the implants surface made of Ti64 alloy erodes easily due to the poor hardness and wear resistance. The debris coming off the worn surface gets mixed with blood and bone cells which causes serious infection in the human body [8,9]. Therefore, over the last two decades, laser surface modification techniques [10–13], especially LSG [3,6], have been used to improve surface hardness and wear resistance of Ti64 alloy. In LSG, higher energy density ($\approx10^{9}Wm^{-2}$) and faster interaction time ($\approx10^{-3}s$) produce ultra-fast cooling rate (10^{5}-$10^{8}Ks^{-1}$) after melting of the surface of materials. This results into very hard, thin and smooth modified surface with amorphous or semi-crystalline microstructure [14,15]. No additional coating material is required in this process and hence, it gives good metallurgical bonding of modified surface layer with the bulk [14]. However, the rapid cooling rates induced by laser heat source develop residual stress in the modified surface area [16–18].

Comparing to other laser surface modification processes [10,11,13], E. Chikarakara et al. reported that LSG offered an outstanding increment (67%) in surface hardness of Ti64 alloy than the untreated

Preprints (www.preprints.org) | NOT PEER-REVIEWED | Posted: 19 March 2018 doi:10.20944/preprints201803.0140.v1

surface [3,6]. Along with improving hardness LSG also enhances wear, corrosion resistance and biocompatibility of the treated surface. However, during LSG, careful selection of the laser parameters such as laser power, beam spot size, scanning velocity, residence time, is prerequisite to achieve the intended properties and avoid surface ablation [8,14]. Experimentally selection of process parameters needs a series of trials where simulation and modelling help optimising process parameters to reduce experimental efforts and also generate theoretical understanding of the process [19–21]. In literature, several FEA models of various laser modification processes of Ti64 alloys were developed to predict temperatures distributions, heat-affected zone and phases present in the modified surface [2,22]. Yilbas et al. and A. Joshi et al. reported the variation of temperature distributions with laser parameters (laser power, beam width, scanning speed, pulse frequency) from FEA analysis for Ti64 alloy [23,24]. However, to the best knowledge of the authors, modelling of LSG for Ti64 alloy is not available in the literature.

Therefore, in this work, a new 3D FEA model of LSG has been developed for the first time using commercial FEA solver ANSYS APDL 17.2. The model can predict the temperature distributions, heating and cooling rates and depth of modified layer of Ti64 alloy. From temperature distributions, the heating and cooling rates has been calculated which were not previously measured in any LSG experimental works. These heating and cooling rates help to predict the possible phase transformation and subsequent surface properties in the modified layer that can be logically justified from theory and literature.

2. Materials and Methods

The modelling of LSG is performed with Ti64/Ti6Al4V alloy which has chemical composition listed in Table 1. LSG represents a transient heat conduction process. The governing equation of this problem is formulated from the 1st law of thermodynamics and Fourier's conduction principle [25] as shown in Equation (1). In this study, Equation (1) expresses the thermal phenomena underpinned in LSG with stationary volumetric heat source.

$$\rho C_P \frac{\partial T}{\partial t} = k\left(\frac{\partial^2 T}{\partial X^2} + \frac{\partial^2 T}{\partial Y^2} + \frac{\partial^2 T}{\partial Z^2}\right) + Q_{laser}(x, y, z), \qquad (1)$$

where, k denotes thermal conductivity, C_P specific heat and ρ density of the material. $Q_{laser}(x, y, z)$ is the intensity of the volumetric heat source, where $X, Y,$ and Z are the global coordinate axes. The intensity distribution of the spherical Gaussian volumetric heat source is expressed by Equation (2) [26,27].

$$Q_{laser}(x, y, z) = \frac{6AP}{\pi\sqrt{\pi}r^3} exp^{\left(\frac{-3\{(x-x_0)^2+(y-y_0)^2+(z-z_0)^2\}}{r^2}\right)}, \qquad (2)$$

where, P is laser power, r is radius of beam, A is the absorptivity and (x_0, y_0, z_o) is the origin of the spherical beam. The heat source in Equation (2) is considered as continuous wave (CW) in TEM_{00} mode of CO_2 laser having 10.6 μm wavelength. The operating laser parameters in this model are laser power, P=300 W, beam radius, r= 0.1 mm (beam radius=beam width/2, where beam width is 0.2 mm) and the residence time, t_R=0.15 ms. Residence time is calculated by dividing the beam diameter with laser scanning speed for the CW laser beam. These laser parameters are adopted from a previous experimental study of LSG [14]. The absorptivity, A of Ti64 alloy is taken 0.4 assuming that laser is absorbed in the flat surface of Ti64 specimen [28]. The initial temperature is considered to be 298 K. Heat loss due to the convection and radiation is ignored as heat source is applied for very brief period (0.15 ms) with small beam width (0.2 mm).

Table 1. Chemical composition of Ti64 alloy in %weight [8].

Element	C	Si	Fe	O	V	Al	Ti
%weight	0.14	0.01	0.16	0.17	3.97	6.36	Balance

Preprints (www.preprints.org) | NOT PEER-REVIEWED | Posted: 19 March 2018 doi:10.20944/preprints201803.0140.v1

Numerical modelling set-up

In this study, a half cylindrical model with 10 mm diameter and 1 mm length has been used and the laser beam is kept stationary, shown in Figure 1, to reduce simulation cost and time. The smaller length of half cylindrical model can be justified by the scale length of thermal diffusion mentioned in A. Issa et al. [29]. The scale length of diffusion $L_D = \sqrt{\alpha t_R}$, where t_R (s) is the residence time of laser heat source and α is the thermal diffusivity of the material. This gives the idea of the maximum length of heat propagation throughout the part. In this case, the scale length is very small (21 μm) due to the short residence time (0.15 ms) and small beam width (0.2 mm). Therefore, 1 mm length of the half cylinder is sufficient in this simulation and can be idealized as semi-infinite solid, which means the local heating cannot affect farther areas of the model.

The 3D solid model of half cylindrical specimen has been created on mechanical APDL of ANSYS 17.2. A single step transient heat transfer analysis has been carried out applying volumetric heat load, because of the large optical absorption coefficient of Ti64 alloy which is 23.25×10^6 m^{-1}. This optical absorption coefficient is calculated from the extinction coefficient of Ti64 alloy for the wavelength of 10.6 μm, as it is considered for the CO_2 laser [30]. The intensity of the volumetric heat source, $Q_{laser}(x, y, z)$ has been calculated from Equation (2) for 300 W laser power, 0.2 mm beam width and 0.15 ms residence time as mentioned earlier.

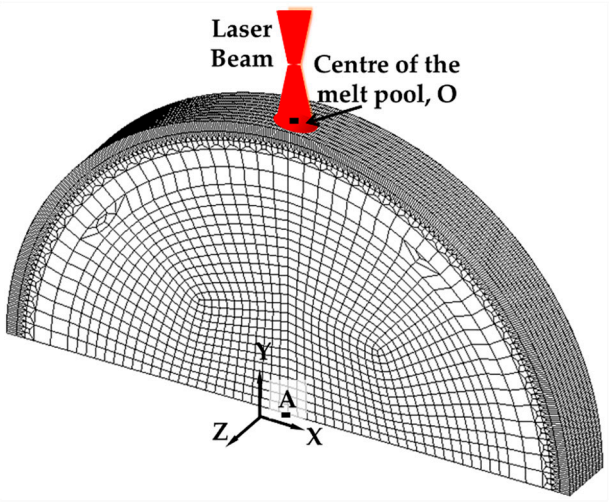

Figure 1. Meshed model of the half solid cylindrical specimen with 10 mm diameter and 1 mm length, where laser beam irradiating on the surface created melt pool; point O is the centre of the melt pool and A is the centre of the half cylindrical specimen.

For the FEA model, Solid 70 element type has been used which has 8 nodes with single degree of freedom as temperature. The surface and sub-surface regions have been meshed finely with gradual coarsening towards the inner region (see, Figure 1) by transitional meshing technique (TMT). TMT helps to reduce the number of elements resulting in increasing efficiency of the simulation process. It also supports in detailed analysis of the surface and subsurface areas where most of the laser material interaction and heating effects are expected to take place based on the scale length, L_D as mentioned earlier. The total numbers of elements for the half cylindrical model are 47060 and the time step size for this transient thermal process has been taken 10^{-6}s. Thermo-physical properties of Ti64 alloy utilised in this simulation is presented in Table 2. Those properties at high temperature above melting point have been kept constant. The approximated temperature isotherm above melting point by this simulation could be overestimated due to the constant properties after melting occurs.

Preprints (www.preprints.org) | NOT PEER-REVIEWED | Posted: 19 March 2018 doi:10.20944/preprints201803.0140.v1

Table 2. Thermo-physical properties of Ti64 alloy as a function of temperature [2,24].

Temperature, K	298	373	573	773	973	1173	1373	1573	1773
Density, kg/m^3	4420	4406	4381	4350	4324	4294	4267	4240	4205
Thermal Conductivity, W/mK	6.8	7.4	9.8	11.8	13.5	20.2	21	23.7	25.8
Specific heat, J/kgK	546	562	606	651	694	734	660	696	732

3. Results and Discussion

In this section, the following results are presented; 1. time-temperature plot, 2. heating and cooling rates and 3. depth of melt pool and HAZ.

3.1. Time-temperature plot

The time-temperature plot, shown in Figure 2, illustrates the temperature variation of the surface with operating time during heating and cooling. From this plot, the peak surface temperature is observed to be 2095 K at 300 W laser power and 0.15 ms residence time. Since, the peak temperature is above the melting point (1933 K) of the Ti64 alloy, it ascertains that a depth of molten or glazed zone must be attained at the selected laser parameters. The time scale in Figure 2 is kept limited up to 0.5 ms because, after this time the cooling curve becomes almost flat, due to the reduction in temperature difference between surface and bulk. However, the surface temperature is observed to cool down to room temperature (298 K) after 1500 ms. If the isothermal temperature lines of melting (1933 K) and β-transus (1268 K; the critical temperature of $\alpha \leftrightarrow \beta$ phase transformation of Ti64 alloy) [31] are superimposed in the time-temperature plot, then the time of phase transformations can also be predicted. For example, at 0.12 ms the surface melting starts and subsequently solidification occurs at 0.18 ms shown in Figure 2. Similarly, when surface reaches β-transus temperature, it is encountered $\alpha \leftrightarrow \beta$ phase transformation at 0.06 ms and 0.35 ms during heating and cooling respectively. By identifying the exact time of the phase transformation and calculating heating and cooling rates for corresponding periods can predict possible phases present in the modified surface [32,33].

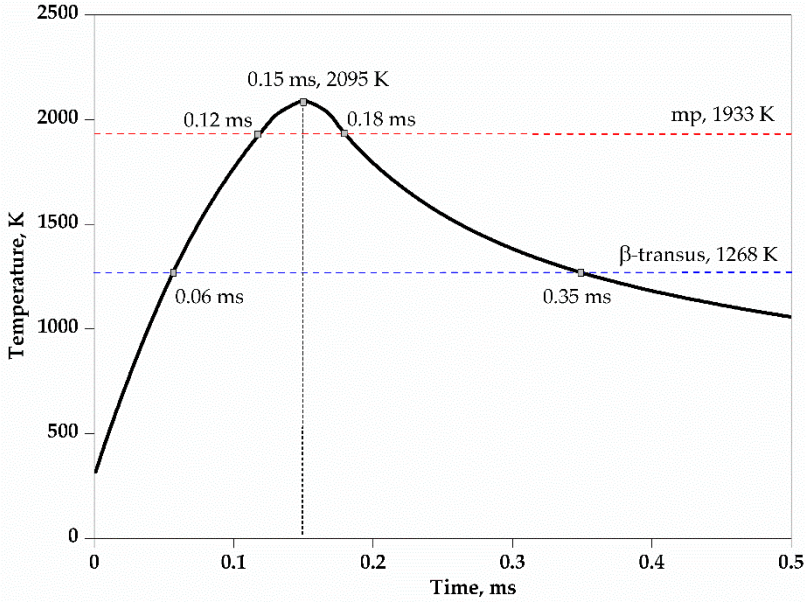

Figure 2. Time-temperature plot of surface at the centre of the melt pool (at point O, see Figure 1) from the Ti64 thermal model for 300W laser power, 0.2mm beam width and 0.15ms residence time. Here, mp is the melting point and β-transus is the critical temperature of $\alpha \leftrightarrow \beta$ phase transformation of Ti64 alloy.

Preprints (www.preprints.org) | NOT PEER-REVIEWED | Posted: 19 March 2018 doi:10.20944/preprints201803.0140.v1

3.2. Heating and cooling rates

The slopes, dT/dt, of the time-temperature plot define the rates of heating and cooling during LSG modelling. The average heating and cooling rates at point O on the surface, are listed in Table 3. In this model, the average heating rate is almost five times higher than the average cooling rate which are 1.19×10^{7} Ks^{-1} and 2.41×10^{6} Ks^{-1} respectively, within the range of initial temperature 298 K and peak surface temperature 2095 K. Such higher heating and cooling rates indicate the presence of amorphous and hard phases in the microstructure of molten zone [8]. In previous studies, it is reported that, due to the short residence or exposure time, cooling rates of 10^{5} to 10^{11} Ks^{-1} can be attained in laser processing and this intensive cooling rates freeze the equilibrium phase transformation resulting into amorphous structure [34]. Initially, the untreated Ti64 alloy is composed of lamella of α and β phases. During LSG, when, the surface temperature rises up and crosses the β-transus, all α phases transformed into β phases. Afterwards, on the onset of cooling all β phase converted into martensitic α phases because of the rapid cooling rate. The molten zone of the surface is assumed to form mixture of amorphous and fine martensitic α, as the presence of refined martensitic α in the laser molten zone due to rapid cooling rates is reported in the literature [8]. However, different shapes of martensitic α grain can be present in the modified zone depending on the range of cooling rates and peak temperatures [35].

Table 3. Average heating and cooling rates on surface at point O, centre of the melt pool for 300 W laser power, 0.2 mm beam width and 0.15 ms residence time.

dT/dt, Ks^{-1}	Average	
Rate of heating	1.19×10^{7}	(298-2095 K, 0.15 ms)
Rate of cooling	2.41×10^{6}	(2095-298 K, 1499.85 ms)

3.3 Depth of Melt pool and HAZ

A temperature isotherm of the transverse cross-section of the specimen at point O (centre of the melt pool) is presented schematically in Figure 3a, where the isotherm shows temperature distribution from surface towards the centre of the half cylindrical specimen up to 60.7 µm depth for time 0.15 ms. The zoomed view of right-hand part the isotherm is presented and scaled in Figure 3b, as the temperature distribution has symmetric distribution along the line OA. The depth of melt pool and HAZ are calculated based on this temperature isotherm. The area having peak temperature above the melting point is referred as melt depth and the area lies above the β-transus, where solid state phase transformation occurs, is designated as HAZ. At 300 W laser power, the calculated depth of melt pool is 22.5 µm whereas the estimated HAZ also has same value of 22.5 µm. The molten zone probably consists of the amorphous and/or refined martensitic α phases depending on the peak temperature and cooling rates. Likewise, the different shapes and sizes of martensitic α and trace amount of β can be retained in HAZ. These amorphous and hard martensitic structure produced from the rapid cooling enhances surface hardness and wear resistance of theTi64 alloy. Therefore, the high energy intensity and shorter residence time of LSG result into significant increase in hardness and wear resistance of treated surface which in turn magnifies the biomedical applicability of laser surface glazed Ti64 alloy.

Preprints (www.preprints.org) | NOT PEER-REVIEWED | Posted: 19 March 2018 doi:10.20944/preprints201803.0140.v1

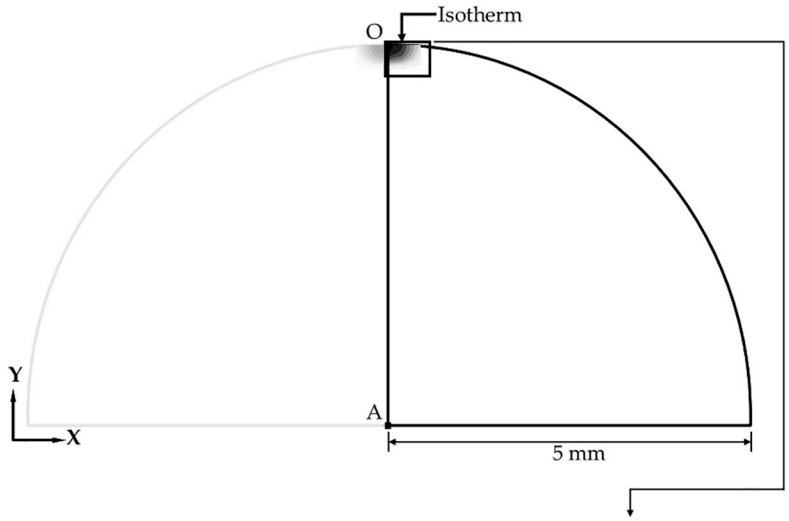

(a)

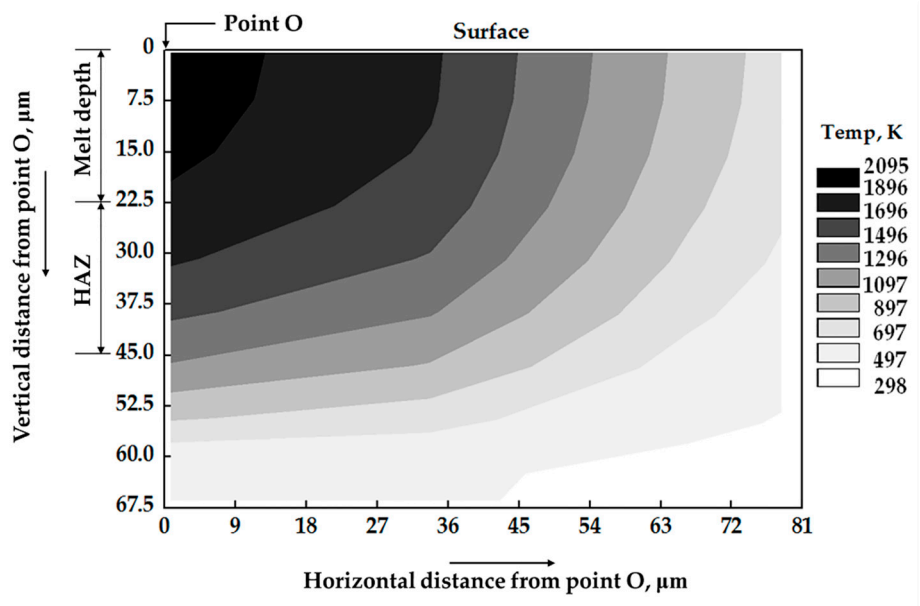

(b)

Figure 3. a) Schematic representation of the temperature isotherm of the transverse cross-section across point O, over the surface of cylindrical specimen at time 0.15 ms for 300 W laser power and 0.2 mm beam width, b) Zoomed view of the right-hand part of the isotherm and is scaled to show depth of melt pool and HAZ.

5. Conclusions

- A 3D FEA thermal model of LSG with cylindrical specimen has been successfully developed for Ti64 alloy. This model can predict the peak surface temperature, depth of modified zone and heating and cooling rates.

- The peak surface temperature, 2095 K is achieved at for 300 W laser powers, 0.2mm beam width and 0.15ms residence time. Both melt depth and HAZ estimated from the temperature isotherm have equal value which is 22.5 µm.

- The average heating and cooling rates are 1.19×10^{7} and 2.71×10^{6} Ks^{-1} respectively calculated from the time-temperature plot which indicate the presence of hard phases in the modified surface layer.

Acknowledgments The work described in this paper has been supported by INTACT project of Erasmus-Mundus (Grant agreement reference: 2013-2829/001-001-EM Action2-Partnerships), and Department of Mechanical Engineering and Aeronautics of City, University of London. The authors are grateful enough to Professor Ranjan Banerjee for the valuable discussion when developing the FEA thermal model.

Author Contributions: Sumsun Naher was involved in developing the concept, reviewing the draft critically, and finally authorized to publish the work. Nusrat Tamanna was involved in editing the draft, Danqing Yin supported in developing FEA model and Israt Rumana Kabir was involved in developing the FEA modelling, data analyses, and documentation of the work.

Conflicts of Interest: The authors declare that they have no conflict of interest.

References

1. Oldani, C.; Dominguez, A. Titanium as a Biomaterial for Implants. In *Recent Advances in Arthroplasty*; Fokter,Dr. S., Ed.; 2012; pp. 149– 162.
2. Yang, J.; Sun, S.; Brandt, M.; Yan, W. Experimental investigation and 3D finite element prediction of the heat affected zone during laser assisted machining of Ti6Al4V alloy. *J. Mater. Process. Technol.* **2010**, *210*, 2215–2222.
3. Chikarakara, E.; Naher, S.; Brabazon, D. High speed laser surface modification of Ti-6Al-4V. *Surf. Coatings Technol.* **2012**, *206*, 3223–3229.
4. Wang, S. H.; Wei, M. D.; Tsay, L. W. Tensile properties of LBW welds in Ti-6Al-4V alloy at evaluated temperatures below 450 °C. *Mater. Lett.* **2003**, *57*, 1815–1823.
5. Van Noort, R. Titanium: the Implant Material of Today. *J. Mater. Sci.* **1987**, *22*, 3801–3811.
6. Chikarakara, E.; Fitzpatrick, P.; Moore, E.; Levingstone, T.; Grehan, L.; Higginbotham, C.; Vázquez, M.; Bagga, K.; Naher, S.; Brabazon, D. In vitro fibroblast and pre-osteoblastic cellular responses on laser surface modified Ti-6Al-4V. *Biomed. Mater.* **2015**, *10*, 015007(1–12).
7. Wally, J. Z., Grunsven, W. V., Claeyssens, F., Goodall, R., Reilly, G. C. Porous Titanium for Dental Implant Applications. *Metals.* **2015**, *5*, 1902–1920.
8. Chikarakara, E. Laser Surface Modiffications of Biomedical Alloys, PhD thesis. Dublin City University, Dublin, Ireland, January **2012**.
9. Parithimarkalaignan, S.; Padmanabhan, T. V. Osseointegration: An update. *J. Indian Prosthodont. Soc.* **2013**, *13*, 2–6.
10. Biswas, A.; Li, L.; Maity, T. K.; Chatterjee, U. K.; Mordike, B. L.; Manna, I.; Majumdar, J. Laser Surface Treatment of Ti-6Al-4V for Bio-Implant Application. *Lasers Eng.* **2007**, *17*, 59–73.
11. Balla, V. K.; Soderlind, J.; Bose, S.; Bandyopadhyay, A. Microstructure, mechanical and wear properties of laser surface melted Ti6Al4V alloy. *J. Mech. Behav. Biomed. Mater.* **2014**, *32*, 335–344.
12. Baloyi, N. M.; Popoola, A. P. I.; Pityana, S. L. Microstructure, hardness and corrosion properties of laser processed Ti6Al4V-based composites. *Trans. Nonferrous Met. Soc. China (English Ed.).* **2015**, *25*, 2912–2923.
13. Bartolomeu, F.; Buciumeanu, M.; Pinto, E.; Alves, N.; Silva, F. S.; Carvalho, O.; Miranda, G. Wear behavior of Ti6Al4V biomedical alloys processed by selective laser melting, hot pressing and conventional casting. *Trans. Nonferrous Met. Soc. China (English Ed.).* **2017**, *27*, 829–838.
14. Aqida, S. N. Laser Surface Modification of Steel, PhD thesis, Dublin City University, Ireland, March **2011**.
15. Kabir, I. R.; Yin, D.; Naher, S. Two dimensional finite element thermal model of laser surface glazing for H13 tool steel. In *19th International ESAFORM Conference on Material Forming*; Chinesta, F.; Abisset-Chavanne, E., Eds.; AIP Conference Proceedings: Nantes, France, 2016; Vol. 110003, pp. 1–6.
16. Tamanna, N.; Crouch, R.; Gavaises, M.; Naher, S. A One-dimensional analysis of the distribution of temperature , stress and strain in the co-axial laser cladding process. In *20th International ESAFORM Conference on Material Forming*; AIP Conference Proceedings: Dublin, Ireland, 2017; Vol. **1896**, p. 040015.
17. Tamanna, N.; Crouch, R.; Kabir, I. R.; Naher, S. An analytical model to predict and minimize the residual stress of laser cladding process. *Appl. Phys. A Mater. Sci. Process.* **2018**, *124*, 1-5.
18. Kabir, I. R.; Yin, D.; Tamanna, N.; Naher, S. Thermomechanical modelling of laser surface glazing for H13 tool steel. *Appl. Phys. A Mater. Sci. Process.* **2018**, *124*, 1–9.
19. Azizpour, M.; Ghoreishi, M.; Khorram, A. Numerical simulation of laser beam welding of Ti6Al4V sheet. *J. Comput. Appl. Res. Mech. Eng.* **2015**, *4*, 145–154.

20. Kumar, C.; Das, M.; Biswas, P. A 3-D finite element analysis of transient temperature profile of laser welded Ti-6Al-4V alloy. In *5th interantional and 26th all India manufacturing technology, design and research conference*; Guwahati, India, 2014; pp. 1–6.
21. Akinlabi, E. T.; Member, I.; Tayob, M. A.; Pietra, F. Experimental and numerical analysis of geometrical properties of laser metal deposited Titanium. In *Proceedings of World Congress on Engineering*; London, UK, 2016.
22. Labudovic, M.; Kovacevic, R. Modelling of the laser surface nitriding of Ti-6Al-4V alloy - analysis of heat transfer and residual stresses. *Inst. Mech. Eng.* **2000**, *215*, 315–340.
23. Yilbas, B. S.; Shuja, S. Z.; Hashmi, M. S. J. A numerical solution for laser heating of titanium and nitrogen diffusion in solid. *J. Mater. Process. Technol.* **2003**, *136*, 12–23.
24. Joshi, A.; Kansara, N.; Das, S.; Kuppan, P.; Venkatesan, K. A study of temperature distribution for Laser Assisted Machining of Ti-6Al-4V alloy. *Procedia Eng.* **2014**, *97*, 1466–1473.
25. Li, J. F.; Li, L.; Stott, F. H. Comparison of volumetric and surface heating sources in the modeling of laser melting of ceramic materials. *Int. J. Heat Mass Transf.* **2004**, *47*, 1159–1174.
26. Goldak, J.; Chakravarti, A.; Bibby, M. A new finite element model for welding heat sources. *Metall. Trans. B* **1984**, *15*, 299–305.
27. Hao, M.; Sun, Y. A FEM model for simulating temperature field in coaxial laser cladding of TI6AL4V alloy using an inverse modeling approach. *Int. J. Heat Mass Transf.* **2013**, *64*, 352–360.
28. Boley, C. D.; Mitchell, S. C.; Rubenchik, A. M.; Wu, S. S. Q. Metal powder absorptivity: modeling and experiment. *Appl. Opt.* **2016**, *55*, 6496.
29. Issa, A.; Brabazon, D.; Hashmi, M. S. J. 3D transient thermal modelling of laser microchannel fabrication in lime-soda glass. *J. Mater. Process. Technol.* **2008**, *207*, 307–314.
30. Ordal, M. A.; Long, L. L.; Bell, R. J.; Bell, S. E.; Bell, R. R.; Alexander, R. W.; Ward, C. A. Optical properties of the metals Al, Co, Cu, Au, Fe, Pb, Ni, Pd, Pt, Ag, Ti, and W in the infrared and far infrared. *Appl. Opt.* **1983**, *22*, 1099.
31. Pederson, R. Microstructure and Phase Transformation of Ti-6Al-4V, Thesis, Luleå University of Technology, Sweden, 2002.
32. Farahmand, P.; Balu, P.; Kong, F.; Kovacevic, R. Investigation of thermal cycle and hardness distribution in the laser cladding of AISI H14 tool steel produced by a high power direct diode laser. In *ASME 2013 International Mechanical Engineering Congress and Exposition*; San Diego, California, USA, 2015; pp. 1–12.
33. Kabir, I. R.; Yin, D.; Naher, S. 3D thermal model of laser surface glazing for H13 tool steel. In *20th International ESAFORM Conference on Material Forming*; AIP Conference Proceedings: Dublin, Ireland, 2017; Vol. 1896, p. 130003.
34. Kurella, A.; Dahotre, N. B. Review paper: Surface modification for bioimplants: The role of laser surface engineering. *J. Biomater. Appl.* **2005**, *20*, 5–50.
35. Broderick, T. F.; Jackson, A. G.; Jones, H.; Froes, F. H. The effect of cooling conditions on the microstructure of rapidly solidified Ti-6Al-4V. *Metall. Trans. A* **1985**, *16*, 1951–1959.